Error Characteristic Analysis of a Standard Model for Geometric Metrology Digital Measuring Instruments

Jing Yu[1,#], Ke-ying Yang[1], Hang Yu[1],Ming Kong[1] and Wei-sheng Zhao[1]

1 College of Metrology Measurement and Instrument, China Jiliang University , Hangzhou, Zhejiang 310018, China
Corresponding Author / Email: yujing88@cjlu.edu.cn, TEL: +86 13735546719, FAX: 0571-86835763

KEYWORDS: Geometric metrology digital measuring instrument, Standard model digital measuring instrument, Point cloud generation error model, Filtering error model

The goals of this study were to devise a standard digital measuring instrument for geometric metrology, analyze its fundamental errors, and provide a crucial basis for subsequent precision measurements. By adhering to preliminary accuracy requirements, we first formulated a theoretical standard model. Additionally, we designed a surface random point generation method and point cloud generation error model for model construction and analysis, respectively. By employing voxel filtering, we successfully reduced the original point cloud density and implemented a filtering error model. The maximum and average errors of each voxel centroid point on one face of the filtered standard model digital measuring instrument were constrained within circular radii of 0.0322 mm and 0.0076 mm, respectively. This established a benchmark for the precise measurement of model dimensions and positional errors. By exploring digital measuring instruments for geometric metrology, this study contributes significantly to the ongoing digital transformation in the field.

NOMENCLATURE

DMI = digital measuring instrument
GMDMI = geometric metrology DMI
SMDMI = standard model DMI
PDMI = physical DMI

1. Introduction

Traditional physical measuring instruments, which are commonly known as "gauges," are measurement devices devoid of amplification or value conversion structures [1]. Examples include gauge blocks, weights, and threaded gauges. In contrast, DMIs derived from metrological digital transformation, whether manifested as datasets, algorithmic software, or physical devices, provide noteworthy advantages such as high precision, robust adaptability, convenient detection and calibration without precision loss, efficient automation during testing, and immunity to wear and external factors.

Within the realm of GMDMIs, there are two primary categories: SMDMIs and PDMIs. GMDMIs, which are specifically tailored for the field of geometric metrology, encompass functions for measuring both size and positional errors. The key distinction between SMDMIs and PDMIs lies in their origins. SMDMIs are derived from a theoretical standard model digital transformation, whereas PDMIs are obtained through the three-dimensional scanning of a physical model. This disparity results in significant differences in error composition and accuracy. In this study, we conducted a comprehensive investigation of SMDMIs for the precise measurement of geometric quantities. This research aligns with China's new development philosophy, leveraging metrological foundations to drive cutting-edge technologies and contribute to efforts in digital transformation, as well as research on value transfer and traceability technology. Precision considerations and practical scanning conditions play crucial roles in the generation of SMDMIs. Following an examination of the appropriate number of measurement points [2–5], we introduce the Monte Carlo method (MCM) [6] to determine model point counts based on initial precision requirements. Subsequently, through voxel filtering, the number of model points is reduced.

2. SMDMI Establishment and Error Analysis

2.1 SMDMI Generation Method and Error Model

The MCM was employed for the development of an SMDMI, which involves the generation of a substantial number of random sample points on the model surface. Subsequent statistical analyses were performed to estimate the initial errors of the simulated SMDMI. When transitioning from a theoretical standard model of a digital instrument to an SMDMI, the initial step requires dividing the surface of the theoretical standard model into m $(m \in \mathbb{N}^+)$ square grids, each with a side length of x_0. The construction of the SMDMI involves the random placement of n $(n \in \mathbb{N}^+)$ points within the area of each grid. Considering the inherently random nature of point selection, it is imperative to calculate and evaluate the generation errors in the

SMDMI, recognizing that a single point is insufficient for a comprehensive correctness assessment. The error of the SMDMI in relation to the theoretical standard model of the digital instrument is determined by evaluating the random deviations of the point cloud's center of gravity.

In Figure 1, a grid of size $x_0 \times y_0$ is used and n $(n \in \mathbb{N}^+)$ points are randomly distributed within the grid. Assuming that this grid is situated in the xoy-plane coordinate system, the coordinates of the randomly placed points are denoted as (x_i, y_i), where $i = 1,2,\dots,n$.

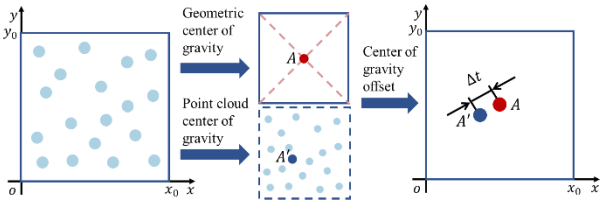

Fig. 1. Illustration of point cloud generation error calculation

Point A represents the centroid of the grid. Based on the regular shape of the grid, the coordinates of point A can be expressed as positions at half the side length away from the grid along the x and y axes. Point A' represents the centroid of the random point cloud. This centroid can be obtained by calculating the average coordinates of all points within the grid. The centroid deviation Δt to be calculated is the distance between A and A', which is given by

$$|\Delta t| = \sqrt{\left(\frac{x_0}{2} - \frac{1}{n}\sum_{i=1}^{n} x_i\right)^2 + \left(\frac{y_0}{2} - \frac{1}{n}\sum_{i=1}^{n} y_i\right)^2} \quad (1)$$

Assuming that the model surface is divided into 1×1 square units, the absolute error between the geometric centroid and point cloud centroid continuously varies with changes in the number of points. Considering the significant randomness involved in this process, to achieve more realistic experimental results, different numbers of points were tested and the experiment was repeated m times. The maximum $(|\Delta t|_{max})$, minimum $(|\Delta t|_{min})$, and average $(|\Delta t|_{avg})$ values of the error were calculated as

$$\begin{cases} |\Delta t|_{max} = max\{|\Delta t|_1, |\Delta t|_2, \dots, |\Delta t|_m\} \\ |\Delta t|_{min} = min\{|\Delta t|_1, |\Delta t|_2, \dots, |\Delta t|_m\} \\ |\Delta t|_{avg} = \dfrac{1}{m}\sum_{j=1}^{m} |\Delta t|_j \end{cases} \quad (2)$$

When $m = 500000$, relevant data plots were obtained based on the variation in the number of points n, as shown in Figure 2.

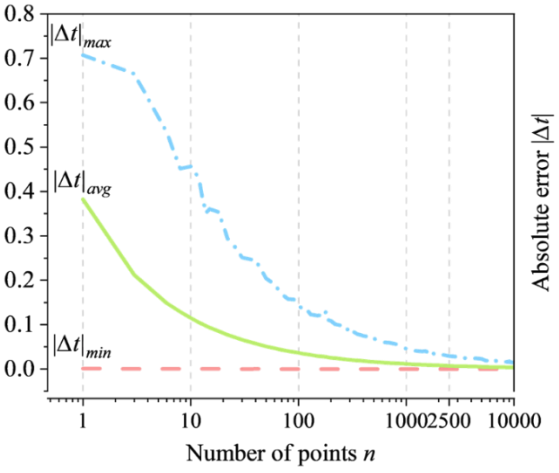

Fig. 2. Absolute errors between the geometric centroid and point cloud centroid with varying numbers of points

In the specified point range, the error distribution was nearly uniform. Consequently, the maximum, minimum, and average absolute errors were segmented into distinct point ranges for polynomial fitting. The selection of the number of points, which is denoted as n, is grounded in the simplicity, intuitiveness, and relative stability of the average value.

$$\begin{cases} |\Delta t|_{\text{avg}} > 0.1 \text{ mm}, n < 14 \\ 0.03 \text{ mm} < |\Delta t|_{\text{avg}} \le 0.1 \text{ mm}, 14 \le n < 150 \\ 0.02 \text{ mm} < |\Delta t|_{\text{avg}} \le 0.03 \text{ mm}, 150 \le n < 350 \\ 0.01 \text{ mm} < |\Delta t|_{\text{avg}} \le 0.02 \text{ mm}, 350 \le n < 1400 \\ |\Delta t|_{\text{avg}} \le 0.01 \text{ mm}, n \ge 1400 \end{cases} \quad (3)$$

Considering $|\Delta t|_{max}$ as an example with $(n_i, (|\Delta t|_{max})_i)$ as data points, where $i = 1,2,\dots,N$, and i is determined by the number of data point sets corresponding to the selected fitting point range, the following polynomial function is obtained:

$$f(n) = a_0 + a_1 n + a_2 n^2 + \cdots + a_k n^k \quad (4)$$

where $a_0, a_1, \dots, a_k$ are the coefficients of the fitting polynomial and k is the degree of the polynomial. Following the fitting process, basic error validation was performed using the residual sum of squares (RSS), total sum of squares (SST), and coefficient of determination (R2). RSS measures the difference between the experimentally obtained and fitted values, SST measures the total variance in the dependent variable, and R2 is used to assess the fitting effect, with a value closer to 1 indicating a better fit. The specific calculation formulas are given in Equation (5).

$$\begin{cases} RSS = \sum_{i=1}^{N} [(|\Delta t|_{max})_i - f(n_i)]^2 \\ SST = \sum_{i=1}^{N} \left[(|\Delta t|_{max})_i - \dfrac{1}{N}\sum_{i=1}^{N} f(n_i)\right]^2 \\ R^2 = 1 - \dfrac{RSS}{SST} \end{cases} \quad (5)$$

Based on the formula for dividing the number of points in Equation (2), separate fittings were performed for $|\Delta t|_{max}$, $|\Delta t|_{min}$, and $|\Delta t|_{avg}$ within different ranges of point numbers. Because randomness is significant when $n < 14$ and the data lack stability, the fitting process began at $n \ge 14$. Because the error of the minimum value is consistently small to the point of being negligible (reaching 10^{-5}), only the final fitting expressions for the maximum and average values are given in Equations (6) and (7), respectively.

During actual processing, the point cloud does not exhibit perfect uniformity. Following voxel grid downsampling, there is a certain range of deviation in the centroid positions. Consequently, when performing compensation, it is imperative to consider a combination of two-dimensional planar and three-dimensional solid errors.

As shown in Figure 3, when calculating the compensation value for two faces, N points are randomly generated on two adjacent surfaces of a cube with a side length of one. The distance from G_b to a specified point is then calculated and the specified point is defined as the midpoint of the boundary line between the two adjacent surfaces of the cube.

As shown in Figure 4, when calculating the compensation value for the three faces, N points are randomly generated on three adjacent faces of a cube with a side length of one. Subsequently, the distance from G_c to a specified point is calculated with the specified point being the intersection point of the three adjacent faces of the cube.

$$f(n_{max}) = \begin{cases} 10^{-10} \times (184549.946n^2 - 45481141.071n + 4017912692.921), 14 \le \text{n} < 150 \\ 10^{-10} \times (4140.576n^2 - 4268357.356n + 1790434569.970), 150 \le \text{n} < 350 \\ 10^{-10} \times (313.603n^2 - 920362.772n + 1068207918.061), 350 \le \text{n} < 1400 \\ 10^{-10} \times (4.476n^2 - 76573.044n + 485143497.739), \text{n} \ge 1400 \end{cases} \quad (6)$$

$$f(n_{avg}) = \begin{cases} 10^{-10} \times (50827.158n^2 - 12276841.309n + 1043681356.184), 14 \le n < 150 \\ 10^{-10} \times (1590.727n^2 - 1288442.422n + 451089265.103), 150 \le n < 350 \\ 10^{-10} \times (83.701n^2 - 231439.984n + 259805686.128), 350 \le n < 1400 \\ 10^{-10} \times (1.025n^2 - 17668.539n + 114109914.551), n \ge 1400 \end{cases} \quad (7)$$

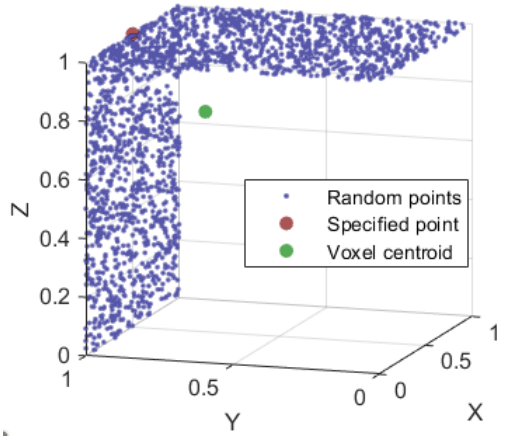

Fig. 3. Illustration of two-face error compensation value calculation

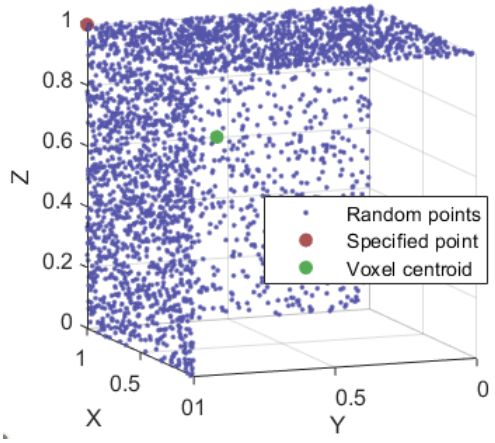

Fig. 4. Illustration of three-face error compensation value calculation

For a cube with a side length of one, various values of N were tested and the error compensation values were calculated over 100,000 iterations, resulting in the data listed in Tables 1 and 2.

Table 1. Two-face edge error compensation values

Number of Points (N)	Two-Face Compensation Value (σ_b)		
	Average Value (σ_{bavg})	Maximum Value (σ_{bmax})	Minimum Value (σ_{bmin})
1000	0.353638	0.375648	0.332952
1500	0.353610	0.371351	0.335879
2000	0.353595	0.370885	0.338435
2500	0.353592	0.367025	0.339355
3000	0.353584	0.366466	0.341562

Table 2. Three-face edge error compensation values

Number of Points (N)	Three-Face Compensation Value (σ_c)		
	Average Value (σ_{cavg})	Maximum Value (σ_{cmax})	Minimum Value (σ_{cmin})
1000	0.577383	0.598288	0.556879
1500	0.577373	0.593839	0.559766
2000	0.577364	0.591577	0.562867
2500	0.577363	0.591094	0.564186
3000	0.577362	0.589592	0.565372

After voxel downsampling with a voxel side length of a on a model with a side length of one, where the average σ_{avg}, maximum σ_{max}, and minimum σ_{min} are affected by changes in model size, the differences between these values are negligible. When performing error compensation on the filtered model, the minimum value σ_{min} can be approximated as the compensation value. Therefore, the compensation value is given by

$$\begin{cases} \sigma_{b\_a} = \sigma_{b\_a\_min} = \sigma_{bavg} \times a - \dfrac{\sigma_{bmax} - \sigma_{bmin}}{2} \\ \sigma_{c\_a} = \sigma_{c\_a\_min} = \sigma_{cavg} \times a - \dfrac{\sigma_{cmax} - \sigma_{cmin}}{2} \end{cases} \quad (8)$$

As a result, the calculated average error values $\sigma_{b\_a\_avg}$ and $\sigma_{c\_a\_avg}$, and maximum error values $\sigma_{b\_a\_max}$ and $\sigma_{c\_a\_max}$ for the two-face and three-face cases after voxel filtering and compensation can be respectively expressed as

$$\begin{cases} \sigma_{b\_a\_avg} = \dfrac{\sigma_{bmax} - \sigma_{bmin}}{2} \\ \sigma_{b\_a\_max} = \sigma_{bmax} - \sigma_{bmin} \end{cases} \quad (9)$$

$$\begin{cases} \sigma_{c\_a\_avg} = \dfrac{\sigma_{bmax} - \sigma_{bmin}}{2} \\ \sigma_{c\_a\_max} = \sigma_{bmax} - \sigma_{bmin} \end{cases} \quad (10)$$

2.2 SMDMI Generation and Error Analysis

when the number of points per square millimeter exceeds 2500, the rate of error change is relatively small and continuing to increase the number of points reduces returns. Additionally, a value of 2500 points per square millimeter provided small and relatively stable maximum and average errors, facilitating subsequent error compensation. Therefore, selecting a point density of $n = 2500\ \text{points/mm}^2$ is optimal. According to the fitting formulas for the maximum and average errors, the calculated values are given by Equations (11) and (12), respectively.

Because an SMDMI is rarely affected by noise, voxel filtering can be applied directly for processing. In this study, the voxel side length was set to $a = 0.2$ mm, dividing the 2500 points in a 1×1 mm plane into 25 smaller planes with dimensions of 0.2×0.2 mm. Because the average error during generation was only 0.0076 mm, the point cloud was considered to be in a nearly uniform state with approximately 100 points in each small plane. Figure 5 presents a schematic of voxel filtering plane division. In this scenario, both the reduced area and point count follow approximately the same pattern.

The centroid error of the small filtered planes can be considered to be approximately equal to the centroid error of the initial plane, as indicated below.

$$f(2500_{max\_1}) = 10^{-10} \times (4.476n^2 - 76573.044n + 485143497.739) = 0.0321686mm \quad (11)$$

$$f(2500_{avg\_1}) = 10^{-10} \times (1.025n^2 - 17668.539n + 114109914.551) = 0.0076345mm \quad (12)$$

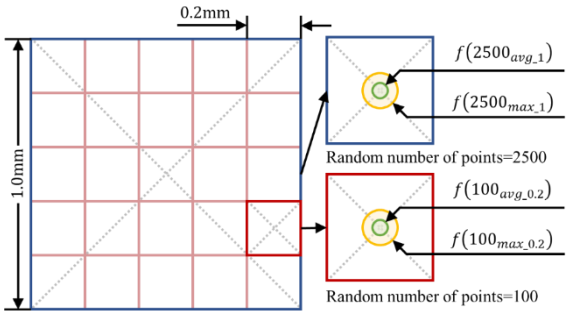

Fig. 5. Voxel filtering plane division diagram

$$f(100_{max\_0.2}) \approx f(2500_{max\_1}) = 0.0321686 \text{ mm} \quad (13)$$

$$f(100_{avg\_0.2}) \approx f(2500_{avg\_1}) = 0.0076345 \text{ mm} \quad (14)$$

Therefore, it can be inferred that the centroid errors of each voxel after voxel filtering were within the area of a circle with a radius of 0.0322 mm with an average error of 0.0076 mm. This also provides the relevant parameters for the subsequent dimension and positional error calculations. The SMDMI measurement results before and after voxel filtering are presented in Figure 6.

In Figure 6, one can see a noticeable reduction in the number points and corresponding decrease in point cloud density. The point cloud density after filtering was only approximately 1% of the original density ($d = 100$ points/mm^2). As a result of this significant reduction in the number of points, the point cloud model at this stage can be processed and stored more efficiently. After voxel filtering, the point cloud exhibits a relatively orderly arrangement, facilitating subsequent analyses and calculations.

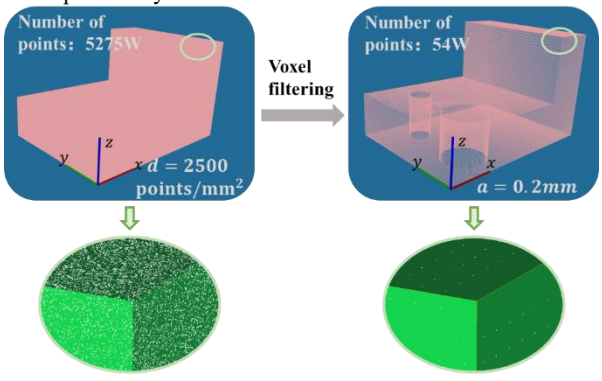

Fig. 6. Experimental measurement results before (left) and after (right) voxel filtering

The results of a comprehensive analysis of the errors in the designed SMDMI model are summarized in Table 6 for a point cloud density $d = 2500$ points/mm^2 and voxel side length $a = 0.2$ mm.

Table 3. Error analysis and filtering effect comparisons

Error Categories		SMDMI	Filtered SMDMI
One Face (σ_a)	Average Value	0.0076 mm	0.0076 mm
	Maximum Value	0.0322 mm	0.0322 mm
Two Faces(σ_b)	Average Value	0.0076 mm	0.0138 mm
	Maximum Value	0.0322 mm	0.0277 mm
Three Faces(σ_c)	Average Value	0.0076 mm	0.0135 mm
	Maximum Value	0.0322 mm	0.0269 mm
Point Cloud Density(d)		2500 points /mm^2	100 points /mm^2

3. Conclusions

In this study, an SMDMI for geometric metrology was designed and its basic errors were analyzed by combining the surface random point generation method and related error models, laying the foundation for precision measurement using subsequent DMIs.

In summary, this study contributes to the generation and error analysis of SMDMIs. In the context of digital transformation, our findings provide valuable insights into both research and engineering practices, as well as a course for the future development of geometric metrology technologies.

ACKNOWLEDGEMENT

The authors gratefully acknowledge the support of Prof. Dongsheng Li and Jinhui Cai, Optical Precision Testing Instrument Laboratory (China Jiliang University).

REFERENCES

1. Liu, K. and Liu, X., “How to distinguish between physical measuring tools and measuring instruments,” China Metrol, Vol. 07, pp. 115, 2020.
2. Liu, H., Cai, J. and Ong, Y.-S., “An adaptive sampling approach for Kriging metamodeling by maximizing expected prediction error,” Comput. Chem. Eng., Vol. 106, pp. 171–182, 2017.
3. Li, B., Feng, P., Zeng, L., Xu, C. and Zhang, J.,“Path planning method for on-machine inspection of aerospace structures based on adjacent feature graph,” Robot. Comput. Integr. Manuf., Vol. 54, pp. 17–34, 2018.
4. Zahmati, J., Amirabadi, H. and Mehrad, V., “A hybrid measurement sampling method for accurate inspection of geometric errors on freeform surfaces,” Measurement, Vol. 122, pp. 155–167, 2018.
5. Zhang, T., Yang, C., Chen, H., Li, S. and Deng, K., “Multi-objective optimization operation of the green energy island based on Hammersley sequence sampling,” Energy Convers. Manag., Vol. 204, 2020.
6. Huang, M., Gou, G., Tang, Z. and Liang. J, “Optimization of coaxiality error detection measurement points based on Monte Carlo,” Modular Mach. Tool. Autom. Process. Technol., Vol. 04, pp. 134–138, 2022.